The Optical Design of HIPO: A High-speed Imaging Photometer for Occultations

Edward W. Dunham

Lowell Observatory, 1400 W. Mars Hill Road, Flagstaff AZ 86001

ABSTRACT

HIPO (High-speed Imaging Photometer for Occultations) is a special-purpose science instrument for use on SOFIA (the Stratospheric Observatory For Infrared Astronomy). HIPO covers the spectral range from the atmospheric UV cutoff at 0.3 microns to the silicon detector limit at 1.1 microns. It is a dual channel imaging photometer using 1Kx1K Marconi CCD47-20 frame transfer CCD detectors. In addition to its science applications, HIPO will be used extensively during performance testing of the SOFIA observatory. The optical design of the instrument includes optimized focal reducing optics for both blue and red channels, pupil viewing optics, and Shack-Hartmann test optics. The imaging performance is excellent, insuring that the instrument will provide a faithful representation of the SOFIA telescope's PSF (Point Spread Function) during test observations.

Keywords: Optical design, Shack-Hartmann, SOFIA

1. INTRODUCTION

HIPO is a two-channel optical high-speed imaging photometer that will be used primarily for observing occultations of stars by solar system objects using SOFIA [1]. It will also be used for applications involving precise photometry, such as measurement of transits of extrasolar planets across their parent stars and asteroseismological observations. All of these applications require precise time-resolved photometry at frame rates up to 50 Hz. The high speed capability and optical flexibility designed into HIPO make it an ideal instrument for performance testing of the SOFIA Observatory. This use has been planned for some time and a few additional design requirements have been added (or tightened) because of this.

Before proceeding to discuss the instrument's design requirements and general configuration, it is important to review the imaging environment in which it will operate. The airborne imaging environment is similar in concept but different in detail from typical ground-based situations. The airborne point spread function (PSF) is essentially unaffected by propagation through the free atmosphere at stratospheric altitude but is instead strongly affected by propagation of starlight through the turbulent shear layer passing over the open telescope cavity. The PSF is affected by turbulence in the telescope cavity ("dome seeing", called "cavity seeing" here), high-speed image motion due mainly to vibration of telescope components (analogous to wind shake), and of course optical imperfections. Our experience in this area is based mainly on the Kuiper Airborne Observatory (KAO) [2]. In the KAO case, all of these factors were comparable in magnitude. Recent test results indicate that the SOFIA telescope optics are of better quality than the initial requirement[3], but image motion at first light is expected to be approximately 2 arcsec rms [4]. The magnitude of the cavity seeing is expected to be lower than the KAO but is not well understood at this time. Wind tunnel aerodynamic measurements [5] together with a numerical wavefront propagation model [6] indicate that the shear layer contribution to the PSF is expected to be strongly wavelength dependent [7] as shown in Figure 1. For completeness, we show both the case for no image motion and the case for long exposures with the expected 2 arcsec rms initial image motion in Figure 1. For the purposes of defining optical design requirements for HIPO we neglect image motion because HIPO will have the ability to time-resolve the motion and measure it separately.

Two important facets of Figure 1 deserve comment here. First, the rapid decrease in image size with wavelength shortward of about 2 microns is due to the growth of a diffraction spike in the center of a broad PSF of light scattered by shear layer turbulence as the wavelength increases to a value comparable to the rms wavefront aberration introduced by the shear layer. It would be desirable to resolve this spike (actually the aberrated telescope PSF), expected to be detectable near 1 micron. Cavity seeing should have a weak wavelength dependence. This is because the turbulent scale size in the cavity is much larger than in the shear layer, so a correspondingly larger wavefront error is needed to have a comparable effect on the PSF size. This wavefront error will be much larger than the wavelength so imaging will be in the geometrical optics limit. Second, it should be pointed out that the increase in expected image size in the blue due to shear layer turbulence implies that the optical requirements on HIPO will be less stringent at shorter wavelengths.

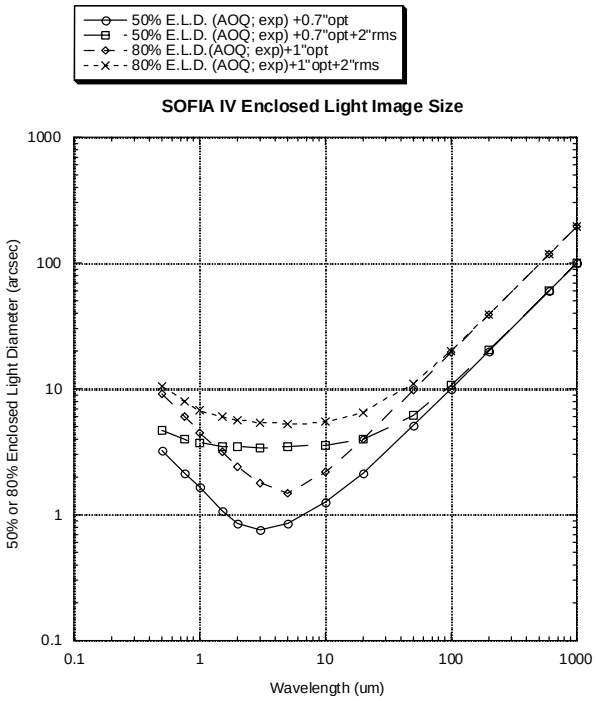

Fig.1: Expected 50% and 80% enclosed light image diameters for SOFIA with and without the anticipated first-light image motion [7]. The image size without image motion is dominated by contributions from shear layer seeing and diffraction with the best image quality in the near-IR being limited by the optical quality and alignment of the telescope. These curves are the ones we pay attention to in the optical design of HIPO since HIPO will be able to time-resolve the image motion. The higher two curves include the expected 2 arcsec rms image motion and are more representative of the expected long exposure first-light imaging performance.

HIPO has been designed to allow co-mounting with FLITECAM, a near-IR imaging spectrograph [8]. This configuration will be useful for certain occultation observations and also for telescope testing. The wavelength dependence shown in Figure 1 clearly indicates that the most critical image quality tests will be made at near-IR wavelengths and a simultaneous measurement from the UV cutoff to 5 microns will be of the greatest value in the effort to discriminate between the effects of shear layer and cavity seeing by virtue of their different wavelength dependence.

The optical layout of the instrument is shown in Figure 2. A window optionally installed at the gate valve location in the telescope allows us to evacuate the volume between the gate valve and the instrument mounting flange if desired. This region will have a very steep temperature gradient and may cause degraded image quality or excess image motion if it is at ambient pressure. The gate valve window will experience wide temperature swings so sapphire was selected because of its strength, high thermal conductivity, low expansion coefficient, and resulting high resistance to thermal shock. The next optical element is a dichroic beamsplitter to reflect the IR band to FLITECAM if FLITECAM is installed. A gold-coated fold mirror finishes the job of directing the beam into FLITECAM. The transmitted optical portion of the beam enters the instrument through a fused silica window and is split by a second dichroic beamsplitter into blue and red spectral regions. The design of the two focal reducers allows the wavelength of the blue/red split to range between 0.4 and 0.65 microns. This beamsplitter can be recoated as needed to optimize the wavelength of the band split for different occultation circumstances. The blue and red collimator-camera focal reducers follow the beamsplitter. The blue side has a single fold mirror that will have an enhanced aluminum coating while the red side has two fold mirrors that will be coated with protected silver.

If FLITECAM is not installed, the IR dichroic beamsplitter will be removed. To accommodate the translation of the optical axis due to this beamsplitter, all the HIPO optical component mounts have compensating shims that will be installed when the beamsplitter is removed. In the same vein if the blue/red beamsplitter is removed the red collimator assembly can be shifted to a second location. We found that it was not necessary to shift the camera lens and detector. The collimator shift introduces a shift in the position of the pupil image, and this has an insignificant effect on the imaging performance of the optics.

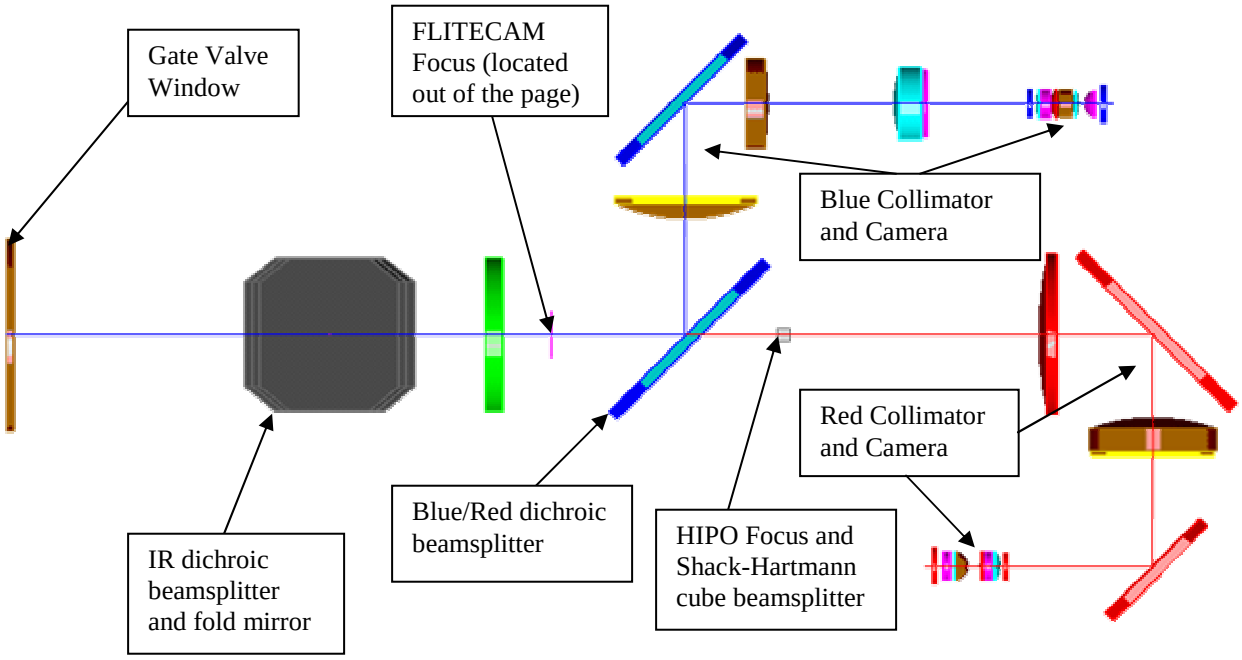

Fig.2: Layout of the HIPO instrument in the case where FLITECAM is co-mounted. The IR dichroic and fold mirror form a periscope bringing the beam up out of the page to line up with the axis of the FLITECAM optics. If FLITECAM is not mounted the IR dichroic beamsplitter will be removed. See text for discussion.

2. OPTICAL REQUIREMENTS

The optical requirements for HIPO are based in part on the demands of occultation work and in part by telescope testing requirements. Each occultation seems to present its own peculiar demands for optimizing data quality. In some cases simultaneous observations with two or three detectors from the UV to IR are desirable while in photon-starved cases a single channel with no loss from reimaging optics is the best approach. The division between the "blue" and "red" channels of HIPO will vary depending on the relative colors of the occulting object and occulted star. This suggests that the operating wavelength ranges of the blue and red sides of HIPO should have considerable overlap. In the test arena, we would like to fully sample the expected PSF, including the ability to detect the presence of the expected small diffraction-limited spike in the PSF at longer optical wavelengths. In addition a Shack-Hartmann capability will be important for independent measurement of the PSF from the telescope optics. A pupil viewing mode is desirable both for optimizing the pupil baffle size and position and for detecting vignetting problems during initial tests of the telescope. Low distortion in at least one optical train is needed to calibrate the chopping secondary performance and offset pointing and tracking capability of the telescope. In addition to these optical requirements we have a series of read rate requirements due to both occultation and telescope testing work that limits the format of the detector.

The requirements we have defined for HIPO, shown in Table 1, are a compromise in which optical system flexibility is used to retain the capability to make all the measurements we currently anticipate. We selected a 1Kx1K frame transfer CCD (the Marconi CCD47-20) operated with two amplifiers in frame transfer mode as a good compromise between field of view and read rate. Operated at a 1 Mpixel/sec read rate we can read out three subframes at 50 Hz and one optimally placed subframe at up to 200 Hz. If we reimage to a scale of 3 pixels per arcsecond we can resolve the expected PSF at most wavelengths and still cover most of the SOFIA focal plane. This scale will probably oversample the PSF at most wavelengths so for occultations we will most likely read the CCD with pixel binning. A bare CCD mode implemented by removing some optical components and relocating the red detector dewar provides maximum throughput at a sacrifice of field of view and also provides the highest spatial resolution for resolving the diffraction-limited spike in the longer wavelength PSF. The requirement that HIPO operate properly on the f/17.5 Perkins 1.8-m telescope reflects our desire to understand the performance of HIPO on a ground-based telescope prior to using HIPO to test SOFIA.

TABLE 1: HIPO OPTICAL DESIGN REQUIREMENTS:

Requirement Category	Requirement or Goal	Status
Wavelength Range	0.35-1.1 µm (0.30-1.1 µm goal)	Goal met
Throughput of reimaging optics	≥ 70% from 0.4 to 0.9 microns	OK
Number of channels	2	OK
Field of View on SOFIA	square, 5.6 arcmin on a side, 8 arcmin diagonal.	OK
Pixel scale on SOFIA	1 "/pixel for occultations, 1/3 "/ pixel for testing (Goal - 0.055 "/ pixel)	Goal met
Optical system	80% enclosed light in 2 pixel box (Goal, 1pixel)	Blue – OK Red – Goal met
	Distortion well characterized for chopper performance evaluation	Red - OK
	Shack-Hartmann capability in one channel, ≥ 20 spots across pupil with X-Y adjustment of Shack-Hartmann MLM	Red – OK.
	Pupil mask with x-y adjustment	OK
	Allow use with 1.8-m Perkins f/17 telescope for instrument test	OK
	Goal - Avoid optics near a focus for maximum photometric precision	Red – Goal met
	Goal - Allow for an evacuated light path to the gate valve	Goal met
	Goal - Allow use of single CCD with no optics for maximum throughput and minimum light loss.	Goal met
	Goal - Provide a pupil imaging mode	Goal met
	Goal - Provide a Focault test capability	Red – Goal met
Co-Mounting	Optional simultaneous mounting with FLITECAM	OK

3. FIRST-ORDER DESIGN DEFINITION

The design requirements just described can be met only with a collimator/camera type of focal reducer with an accessible pupil image. Refractive optics were selected to combine good control of field aberrations with high throughput. The collimator focal length and pupil size is a compromise between imaging performance (arguing for a longer focal length), and size and cost of elements together with size, weight, and structural stability of the instrument (all arguing for a shorter focal length). We settled on a pupil diameter of 20 mm for the SOFIA telescope, providing a reasonable instrument size (with fold mirrors) and allowing use of 25 mm filters. For the Perkins application, considering the effects of mechanical crowding and steepness of the beams in the vicinity of the pupil, field-dependent pupil aberration, and allowing for mounting hardware, 28 mm filters provide a little more margin against vignetting.

Initial design guidance was found in Smith [9] and the ZEBASE design examples available with ZEMAX [10]. Fischer and Tadic-Galeb [11] provided valuable advice, particularly in the manufacturability of the design. The optical design was optimized using ZEMAX [10] for SOFIA but with the elements sufficiently oversized to allow unvignetted operation with the Perkins telescope. The image quality when operated at *f*/17.5 is about the same as for SOFIA at the field center but is not as good at the field corners. However, the image quality at the corners of the field when used on the Perkins telescope is still significantly better than the seeing so additional improvement to the design was not necessary.

4. DETAILED DESIGN DISCUSSION

4.1 Glass selection

Glass selection for the blue side optics was straightforward, being circumscribed by the desire to have good transmission down to the atmospheric UV cutoff at 0.3 microns. This requirement effectively restricts the glass selection to CaF_2 and fused silica.

There is much more flexibility in glass selection for the red side optics. The primary important aspect is in the CaF_2 and KzFS4 doublets in the collimator and camera lenses. This glass pair gives excellent color correction, though both are expensive materials. BaF_2 is somewhat superior to CaF_2 for the positive elements but its additional cost and fabrication difficulty outweighed its optical benefits. The glass selection was guided by the process for design of a three-lens apochromat described by Herzberger and Salzberg [12] and Kinslake [13], but with a good deal of trial and error as well.

4.2 Pupil issues

The pupil image will be used in four ways by HIPO, none of them requiring a high quality pupil image. First, a stop at this location will serve as an effective stray light baffle. The position of this stop is manually adjustable. Second, the pupil provides a convenient location for filters. Third, a pupil viewing mode will be used to align the pupil stop and to check for obvious vignetting by a misbehaving telescope cavity door during early tests of the telescope. Fourth, the lenslet module for the Shack-Hartmann test optics will be located close to the pupil image. This test will be carried out on an isolated bright star located near the center of the field of view, so small field-dependent pupil aberrations are acceptable. The pupil size is weakly dependent on field position, growing about 3% from the on-axis field to the corner field. The collimation and pupil image centering are well controlled.

4.3 Blue side reimaging optics

The blue side focal reducing optics meet the image quality requirement in Table 1 while also meeting the goal of transmitting down to the atmospheric UV cutoff at 0.3 microns. To achieve this transmission goal the lenses are all either fused silica or CaF_2. Because of the similar index of these two materials the lens curvatures tend to be steep and alignment will be a little tricky. It was found that a single asphere on the surface closest to the pupil allowed the spherical aberration to be corrected there independent of the rest of the lens, thereby releasing the other surfaces to correct for other aberrations. This significantly improved the performance of the lens. Distortion was not constrained in the design optimization because low distortion is only needed in one of the channels and it is easier to achieve with the wider available glass selection on the red side. Similarly the blue side optics do not meet the goal of avoiding optics near a focus, the first element of the collimator being in effect a field lens. Finally, the Shack-Hartmann mode is built into the red side optics only. The as-built prescription for the blue side reimaging optics is given in Table 2 and the performance of the as-built blue side focal reducing optics with reoptimized spacings is shown in Figure 3 below.

TABLE 2: HIPO BLUE SIDE OPTICAL PRESCRIPTION:

Surface Name	Radius (mm)	Convex (CX) Concave (CC)	Thickness (mm)	Glass
TELESCOPE FP	Infinity	- - -	24.84953	
FIELD LENS	187.7962	CX	25.14	SILICA
	1779.461	CX	95.19047	
FOLD MIRROR	Infinity	Plano	70.77284	MIRROR
COLL 2	126.434	CC	15.14	SILICA
	333.735	CX	130.4296	
COLL 3	115.226	CX	15.2	SILICA
	50.526	CC	1.697701	
COLL 4	51.6	CX	18.04	CAF2
	Infinity	Plano	105.1274	
FILTER	Infinity	Plano	5	SILICA
	Infinity	Plano	1	
PUPIL	Infinity	- - -	2	
CAMERA 1	38.935	CX (asphere)	9.096	CAF2
	26.602	CX	0.29129	
CAMERA 2	26.181	CC	4.1	SILICA
	36.684	CC	0.2029127	
CAMERA 3	17.401	CX	13.1	CAF2
	34.862	CX	2.682564	
CAMERA 4	21.506	CC	4.04	SILICA
	14.701	CC	4.398434	
CAMERA 5	34.349	CX	7.12	CAF2
	34.35	CX	5.221734	
CAMERA 6	14.814	CX	5.03	SILICA
	14.203	CC	13.91	
WINDOW	Infinity	Plano	4	SILICA
	Infinity	Plano	7.79	
FOCAL PLANE	Infinity	Plano		

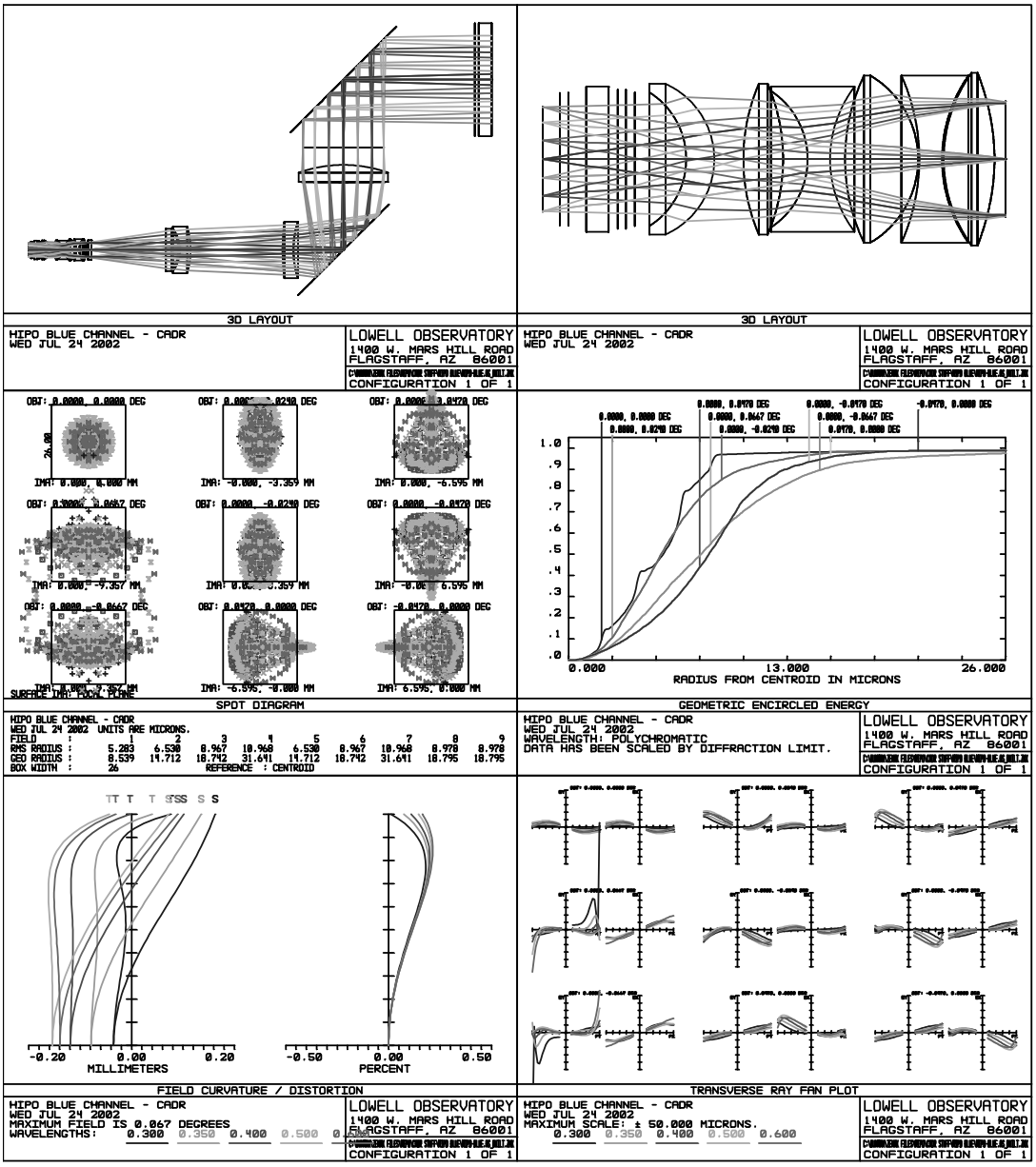

Fig.3: Performance summary of the HIPO blue side reimaging optics.

Upper left: The instrument entrance window is at the right followed by the dichroic beamsplitter, the four-element collimator with embedded fold mirror, and the camera lens. The last element of the collimator is a CaF_2 positive element, the others being fused silica.

Upper right: The camera lens layout from pupil plane (right) to detector (left). The camera elements are alternating positive CaF_2 and negative fused silica elements. The first surface in the camera is an even asphere.

Middle left: Spot diagrams shown with 26 micron (2 pixel) boxes. The fields, left to right, then top to bottom are center, halfway to edge, edge, and corner, followed by off-axis fields in other orientations.

Middle right: Enclosed light curves for the several fields. Note that 80% enclosed light falls within a 1 pixel radius for all fields.

Lower left: The left plot shows longitudinal focus error against field position for tangential and sagittal planes for five wavelengths. The right plot shows percent distortion against field position.

Lower right: Ray aberration fans for the same nine fields shown in the spot diagram.

4.4 Red side reimaging optics

The red side focal reducing optics design meets the image quality goal in Table 1 across the band from 0.4-1.0 microns. To achieve this we allowed the design to develop some steep curvatures and accept the associated effort required for alignment. As with the blue side optics we found that a single asphere on the surface closest to the pupil improved the performance of the lens. The KzFS4/CaF_2 contact doublet in the camera lens is coupled with Q2-3067 optical couplant to allow for the thermal expansion mismatch of the two glasses. Distortion was constrained in the design optimization and is very low, particularly at 0.55 microns. The optics are all relatively far from a focus, meeting the goal in Table 1 for precision photometry. The Shack-Hartmann mode is built into the red side optics and is described in Section 4.7. A simple knife-edge located near the beamsplitter for the Shack-Hartmann test allows a Focault test to be carried out using the red side pupil viewing optics. The as-built prescription for the red side reimaging optics is given in Table 3 and the performance of the as-built red side focal reducing optics with reoptimized spacings is shown in Figure 4 below.

TABLE 3: HIPO RED SIDE OPTICAL PRESCRIPTION:

Surface Name	Radius (mm)	Convex (CX) Concave (CC)	Thickness (mm)	Glass
INT FP	Infinity	- - -	271.2577	
COLLIMATOR 1	-409.595	CX	20.1	SSKN8
	Infinity	Plano	99.05744	
FOLD MIRROR	Infinity	Plano	86	MIRROR
COLLIMATOR 2	197.87	CX	10.06	N-KZFS4
	97.126	CC	1.730083	
COLLIMATOR 3	97.242	CX	30.09	CAF2
	1950.001	CX	113.42	
FOLD MIRROR	Infinity	Plano	150.428	MIRROR
FILTER	Infinity	Plano	5	N-BK7
	Infinity	Plano	1	
PUPIL	Infinity	- - -	3	
CAMERA 1	26.6	CX (asphere)	6.082	CAF2
	201.246	CC	4.50819	
CAMERA 2	44.885	CC	3.01	N-KZFS4
	60.385	CC	0	Greased pair
CAMERA 3	60.385	CX	8.17	CAF2
	39.289	CX	11.58057	
CAMERA 4	15.997	CX	4.04	N-BK7
	15.639	CC	3.827668	
CAMERA 5	24.446	CX	7.15	SSKN8
	212.201	CX	5.928591	
CAMERA 6	18.391	CC	3.04	SSKN8
	80.113	CC	7.943189	
WINDOW	Infinity	Plano	4	SILICA
	Infinity	Plano	7.79	
FOCAL PLANE	Infinity			

4.5 Tolerances, optomechanical issues, and fabrication experience

The HIPO optics were fabricated by Optimax. Fabrication of the powered HIPO optics is complete including antireflection coating. With the exception of the large sapphire gate valve window, the windows, fold mirrors and beamsplitters have been delivered but have not yet been coated. The manufacturing tolerances of the reimaging optics were not in general difficult to meet. Almost all surfaces are well within their required tolerances in every respect. The thicknesses are almost all thicker than the nominal value but are within the tolerance allowed. The aspheres, as always, took longer to produce than the spherical surfaces but are also well within their tolerances. The main fabrication difficulty was the tendency for the small KzFS4 element in the red camera lens to chip.

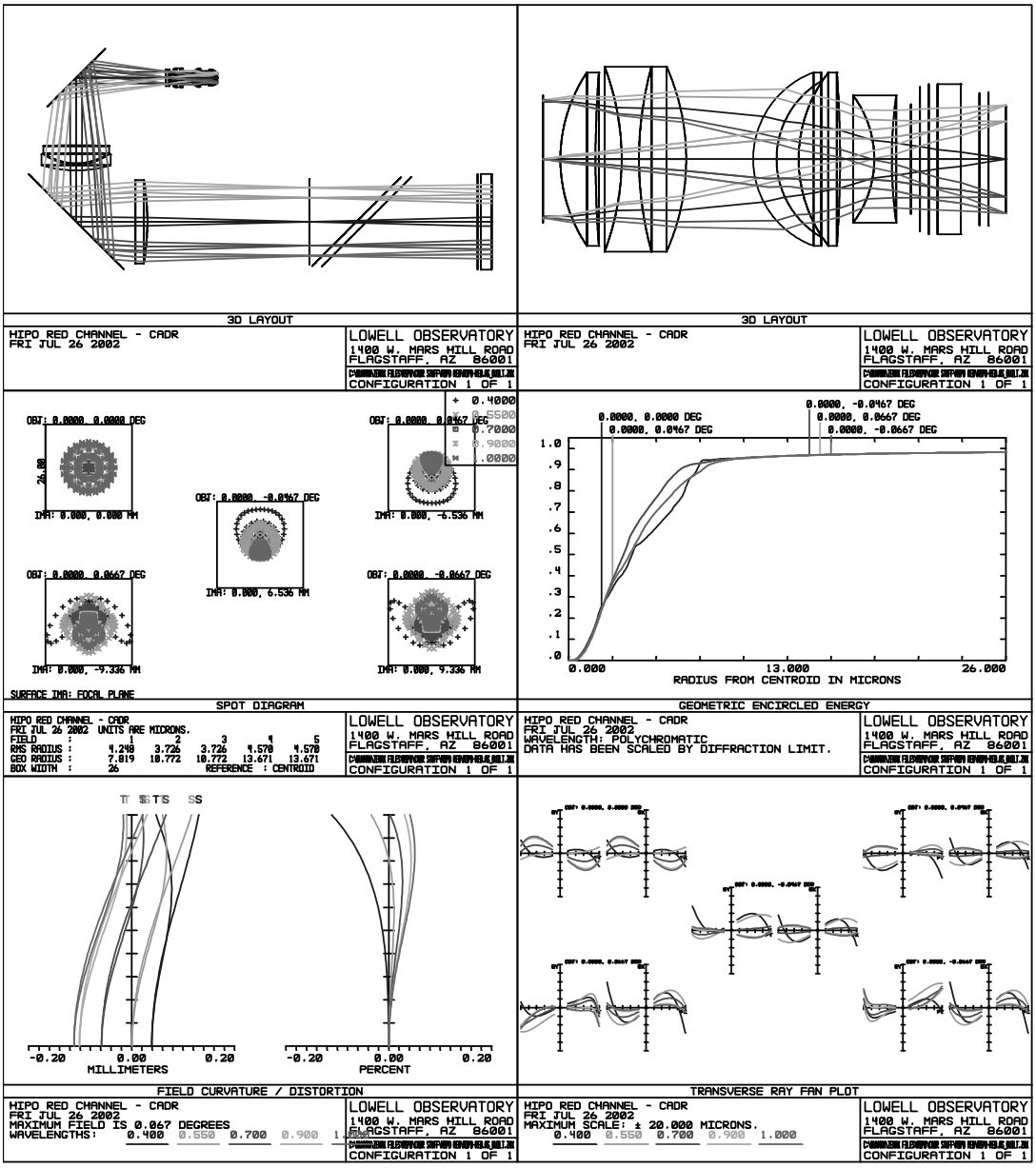

Fig.4: Performance summary of the HIPO red side reimaging optics.

Upper left: The instrument entrance window is at the right followed by the dichroic beamsplitter, telescope focal plane, three-element collimator with embedded fold mirror, a second fold mirror, filter, and the camera lens. The last doublet of the collimator is a KzFS4/CaF_2 pair.

Upper right: The camera lens layout from pupil plane (left) to detector (right). The first camera element is CaF_2 followed by a KzFS4/CaF_2 pair. The first surface in the camera is an even asphere. The steep meniscus is BK7 and the last two elements are SSKN8.

Middle left: Spot diagrams shown with 26 micron (2 pixel) boxes. The fields are center, edge, and corner.

Middle right: Enclosed light curves. Note that 80% enclosed light falls within a 1/2 pixel radius for all fields.

Lower left: The left plot shows longitudinal focus error against field position for tangential and sagittal planes for five wavelengths. The right plot shows percent distortion against field position. Note the very low distortion at 0.55 microns wavelength.

Lower right: Ray aberration fans for the same fields shown in the spot diagram.

The mounting tolerances for the collimator elements are not very tight. The tightest are the relative alignment of the lenses in the final doublets in each collimator, but the overall alignment of each doublet is quite loose. We expect to be able to use what Yoder [14] calls the "drop-in" mounting arrangement for these elements with the possible exception that the final doublet may be located by surfaces in contact with the polished surfaces of the lenses. The lenses will be held in place along the optical axis by spring washers to insure that some force is always applied but to allow for thermal expansion.

The alignment tolerances on the camera elements are generally tighter. We found that centering adjustments of two of the negative elements (2 and 4) on the blue side and one element (6) on the red side were effective compensators for tilt errors in these and other components as well as for decenter errors in other elements. Given the compensating effect of these lenses the acceptable decenter and tilt errors on the other camera lens elements can easily be met with retainers in contact with the polished lens surfaces.

The lenses need to operate under temperatures down to about −10C and up to room temperature, and need to survive temperatures up to 160C when SOFIA is locked up in a very hot climate. The lens cells are all aluminum, so the hot temperatures do not pose a survival threat, rather the cold temperatures are the main concern.

The HIPO lenses and dewar windows were coated by Thin Film Labs in separate coating runs for the blue and red optics. Only one coating run was needed for the blue optics because of the similar index of CaF_2 and fused silica, but a low-index and high-index pair of runs was needed for the red side optics. The combined transmission curves of the HIPO lenses and dewar windows based on measurements of witness samples are shown in Figure 5.

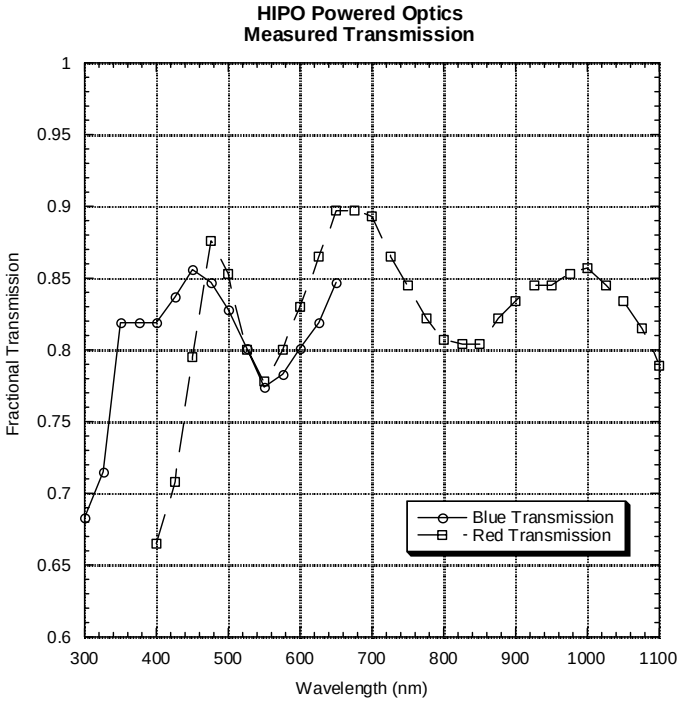

Fig.5: Transmission curves for the blue and red side optics based on measurements of witness samples. These curves include all the powered optics and dewar windows but exclude the currently uncoated mirrors, beamsplitters and gate valve and instrument windows. The latter two windows and the AR coating on the IR dichroic beamsplitter will be the most troublesome coatings due to the wide wavelength range they must encompass.

Coating of the sapphire gate valve window will be an exercise in compromise. The window needs to operate over the 0.3 to 5 micron range and no multilayer AR coat will be effective over such a wide wavelength range. Most likely it will be coated for the IR part of the range, with higher order interference effects causing some optical bands to show good transmission characteristics with others being no better than the uncoated substrate. The fused silica instrument window

and the second surface of the FLITECAM dichroic reflector also must operate over a wide wavelength range, from 0.3 to 1 micron. This will be less problematic but will also require some compromise.

4.6 Pupil viewing optics

The pupil viewing optics consist of a classic field lens, collimator, and camera focal reducer made with stock optics. This lens assembly will be mounted in a cell that will replace the camera lens. Since we do not anticipate using this mode often, lens replacement will be a manual operation. The same lenses are used for both the blue and red side pupil viewing optics since there is no need for UV pupil viewing capability. As shown in Table 4, the lens spacings are slightly different for the two pupil viewing lens assemblies and the performance of the blue side is poorer than for the red side. In both cases the plano side of the singlet field lens faces the pupil image formed by the main collimator lens set and both BK7-SF2 doublets have their BK7 elements facing the field lens and their SF2 elements facing the CCD.

TABLE 4: HIPO PUPIL VIEWING OPTICAL PRESCRIPTIONS AND PERFORMANCE:

Lens or Surface	Blue Side Data (B filter)	Red Side Data (R filter)
Pupil Image		
	5.00 mm	5.00 mm
Opto Sigma 011-1990		
	27.83 mm	28.27 mm
Opto Sigma 026-0460		
	10.74 mm	12.36 mm
Opto Sigma 026-0160		
	6.21 mm	7.06 mm
Window		
Enclosed Light Diameter (at secondary mirror)	50% in 6.8 mm, 80% in 14 mm	50% in 4.6 mm, 80% in 7.0 mm

4.7 Shack-Hartmann optics

The Shack-Hartmann test optics use the concept described by Pernechele, *et al.* [15] that allows any collimator/camera focal reducer to be used for a Shack-Hartmann test. A negative lens is located near the pupil and lenslet module to compensate for the focusing effect of the lenslets. A judicious choice of lenslet focal length rescales the pupil image to fit the detector format. The ideal lenslet configuration was not available as a stock item in the AOA catalog so two different lenslets were selected together with their corresponding stock negative lenses as shown in Table 5. One configuration gives finer sampling across the pupil but the pupil image is slightly larger than the detector. The other configuration comfortably fits the pupil image on the detector but has coarser sampling. Both configurations also include an R filter to reduce the effect of chromatic aberration from the singlet lenses. For calibration purposes a pinhole image at the telescope focal plane can be projected into the Shack-Hartmann optical system by means of the cube beamsplitter shown in Figure 2.

TABLE 5: HIPO SHACK-HARTMANN ELEMENTS:

Component	Fine Sampling	Coarse Sampling
Beamsplitter	Melles Griot 03BSC005, 12.7mm cube beamsplitter	
Lenslet Module	AOA 0497-97-H	AOA 1060-206-S
Negative Lens	Opto Sigma 012-0160 singlet	Melles Griot 01LQT012 singlet

4.8 Retroreflection optics

We have incorporated the ability to project a pinhole image located at the telescope focal plane back out into the telescope. This uses the other side of the same cube beamsplitter used for the Shack-Hartmann test calibration pinhole. A small concave spherical mirror with radius equal to the separation between the secondary and the focal plane optionally located in the central obscuration area of the secondary mirror will intercept part of this expanding spherical wavefront and form an image of the pinhole also located at the telescope focal plane. This image will move under the influence of motions of the secondary mirror (either intentional or unintentional) and also due to aero-optical effects in the cavity and Nasmyth tube. We will distinguish between these effects by making use of accelerometers mounted on the optical elements of the telescope during the test program.

ACKNOWLEDGEMENTS

Thanks are due to Jochen Horn, Dan Clemens, Jim Burge, Harland Epps, and Jim Elliot for helpful tips and valuable discussions. This work was supported under USRA SOFIA subcontract 8500-98-003.

REFERENCES

1. Dunham, E.W., J.L. Elliot, and B.W. Taylor, "HOPI – A High-speed Occultation Photometer and Imager for SOFIA", *Proc. SPIE* **4014**, 76-84, 2000.
2. Elliot, J.L., E.W. Dunham, R.L. Baron, A.W. Watts, S.E. Kruse, W.C. Rose, and C.M. Gillespie, Jr., "Image Quality on the Kuiper Airborne Observatory. I. Results of the First Flight Series", *P.A.S.P.*, **101**,. 737-764, 1989.
3. Erickson, E.F., Private Communication, 2002.
4. Erickson, E.F. and E.W. Dunham, "Image Stability Requirement for the SOFIA Telescope", *Proc. SPIE* **4014**, 1-12, 2000.
5. Rose Engineering and Research, Inc., "SOFIA – Conceptual Door Design and Aero-Optics Wind Tunnel Test", Final Report for NASA Subcontract SC-065, submitted to Sverdrup Technology, Inc. at NASA Ames Research Center, March 1996. Available from the SOFIA Project Office library.
6. SY Technology, Inc., "SOFIA Aero-Optic Analysis". Available from the SOFIA Project Office library.
7. Dunham, E.W., "Predicted SOFIA Image Size vs. Wavelength", TN-EWD-005.R4, 2002. Available from the SOFIA Project Office library.
8. Horn, J.M.M., *et al.*, "FLITECAM – A near-infrared camera for test and science applications on SOFIA", *Proc. SPIE* **4014**, 64-74, 2000.
9. Smith, W.J., "Modern Lens Design", Optical and Electro-Optical Engineering Series, McGraw-Hill, Second Edition, 1992.
10. Focus Software, "ZEMAX Optical Design Program", Tucson, AZ., 2002.
11. Fischer, R.E., and B. Tadic-Galeb, "Optical System Design", McGraw-Hill, 2000.
12. Herzberger, M. and C.D. Salzberg, "Refractive Indices of Infrared Optical Materials and Color Correction of Infrared Lenses", *JOSA*, **52**, 420-427, 1962.
13. Kingslake, R. "Lens Design Fundamentals", Academic Press, 1978.
14. Yoder, P.R., "Opto-Mechanical Systems Design", Second Edition, Marcel Dekker, 1993.
15. Pernechele, C., F. Bortoletto, D. Fantinel, and E. Giro, "Afocal Shack-Hartmann Screen for and Instrument with an Accessible Pupil", *PASP* **112**, 996-1000, 2000.